

# Ultrahigh Thermoresistant Lightweight Bioplastics Developed from Fermentation Products of Cellulosic Feedstock


Aniruddha Nag, Mohammad Asif Ali, Hideo Kawaguchi, Shun Saito, Yukie Kawasaki, Shoko Miyazaki, Hirotohi Kawamoto, Deddy Triyono Nugroho Adi, Kumiko Yoshihara, Shunsuke Masuo, Yohei Katsuyama, Akihiko Kondo, Chiaki Ogino, Naoki Takaya, Tatsuo Kaneko,\* and Yasuo Ohnishi\*

Production of bioplastics from renewable biological resources is a prerequisite for the development of a circular and sustainable society. Current bioplastics are mostly heat-sensitive aliphatic polymers, requiring thermoresistant aromatic bioplastics. Herein, 3-amino-4-hydroxybenzoic acid (AHBA) and 4-aminobenzoic acid (ABA) are produced from kraft pulp, an inedible cellulosic feedstock, using metabolically engineered bacteria. AHBA is chemically converted to 3,4-diaminobenzoic acid (DABA); subsequently, poly(2,5-benzimidazole) is obtained by the polycondensation of DABA and processed into an ultrahigh thermoresistant film. The copolymerization of DABA with a small amount of ABA dramatically increases the degradation temperatures of the resulting films (over 740 °C) to yield the most thermoresistant plastic on record. Density functional theory calculations indicate that the incorporation of ABA strengthens the interchain hydrogen bonds between aromatic imidazole rings. Thus, an alternative organic molecular design is proposed for thermoresistant plastics without using heavy inorganics, although continuous aromatic heterocycles are widely considered ideal for polymer thermoresistance. This innovative macromolecular design increases thermoresistance and can be widely applied to well-processable plastics for the production of lightweight materials and is expected to contribute to the development of a more sustainable society.

## 1. Introduction

The production of biobased polymers using renewable materials has garnered significant attention from researchers in recent decades to achieve the United Nation's Sustainable Development Goals (SDGs).<sup>[1]</sup> Global demand for plastics has reached 360 million tons per year, less than 1% (2.11 million tons) of which were produced from renewable resources such as biomass in 2019.<sup>[2]</sup> One reason for the low production of biobased plastics is the low performance of biobased plastics, especially in terms of heat resistance, and it should be improved for the wider use of biobased plastics.<sup>[3]</sup> In addition, most conventional monomers of biobased plastics, such as lactic acid for poly(lactic acid) (PLA) and succinic acid for poly(butylene succinate), are produced by the fermentation of edible sugars and starch, which creates another problem, competition with limited food resources.<sup>[4]</sup> Therefore,

Dr. A. Nag, Dr. M. A. Ali, H. Kawamoto, Prof. T. Kaneko  
Graduate School of Advanced Science and Technology  
Energy and Environment Area  
Japan Advanced Institute of Science and Technology (JAIST)  
1-1 Asahidai, Nomi, Ishikawa 923-1292, Japan  
E-mail: kaneko@jaist.ac.jp  
Prof. H. Kawaguchi, K. Yoshihara, Prof. A. Kondo  
Graduate School of Science  
Technology and Innovation  
Kobe University  
1-1 Rokkodai, Nada, Kobe 657-8501, Japan

 The ORCID identification number(s) for the author(s) of this article can be found under <https://doi.org/10.1002/adsu.202000193>.

© 2020 The Authors. Advanced Sustainable Systems published by Wiley-VCH GmbH. This is an open access article under the terms of the Creative Commons Attribution-NonCommercial-NoDerivs License, which permits use and distribution in any medium, provided the original work is properly cited, the use is non-commercial and no modifications or adaptations are made.

DOI: 10.1002/adsu.202000193

Dr. S. Saito, Prof. Y. Katsuyama, Prof. Y. Ohnishi  
Graduate School of Agricultural and Life Sciences  
The University of Tokyo  
1-1-1 Yayoi, Bunkyo-ku, Tokyo 113-8657, Japan  
E-mail: ayasuo@mail.ecc.u-tokyo.ac.jp

Dr. Y. Kawasaki, Dr. S. Masuo, Prof. N. Takaya  
Faculty of Life and Environmental Sciences  
University of Tsukuba  
Tsukuba, Ibaraki 305-8572, Japan

S. Miyazaki, D. T. N. Adi, Prof. A. Kondo, Prof. C. Ogino  
Graduate School of Engineering  
Kobe University  
1-1 Rokkodai, Nada, Kobe 657-8501, Japan

Prof. Y. Katsuyama, Prof. Y. Ohnishi  
Collaborative Research Institute for Innovative Microbiology  
The University of Tokyo  
1-1-1 Yayoi, Bunkyo-ku, Tokyo 113-8657, Japan

inedible renewable feedstocks have been getting much attention in the production of biomonomers using genetically engineered microorganisms.<sup>[5]</sup> Plant-derived cellulosic feedstocks, comprised of cellulose, hemicellulose, and lignin, are attractive alternatives to petroleum-derived feedstocks due to being inedible, renewable, and the most abundant feedstocks in the biosphere.<sup>[6,7]</sup> Kraft pulp, corn stover, wheat straw, and sugarcane bagasse are examples of cellulosic feedstocks. Many attempts have been made to use these inedible feedstocks as a carbon source for the fermentative production of various compounds.<sup>[8–10]</sup>

In recent years, polymers containing ring moieties derived from saccharides and lignin have attracted the attention of researchers for their enhanced thermomechanical performances as compared to those of aliphatic biobased polymers.<sup>[11]</sup> Currently manufactured bioplastics, such as polyamide 11, poly(glycolic acid), polyhydroxyalkanoates, and PLA, are mainly composed of aliphatic polymers, which limits their applications in the field of engineering due to their low levels of thermal resistance.<sup>[12–14]</sup> Petroleum-derived high thermoresistant polymers, such as poly(ether ether ketone) (PEEK), polyazoles, polyimides, aramids, and liquid crystalline polymers (LCPs), are mainly composed of aromatic backbones.<sup>[15]</sup> Except for lignin with phenylpropanoid units, there are no such aromatic biopolymers in nature.<sup>[8,16]</sup> Some researchers have attempted to use lignin as a polymer material, but lignin biomolecules are difficult to control structurally, which restricts their application in industry.<sup>[17–19]</sup> Therefore, aromatic biomolecules can be good candidates for use as renewable starting materials in the synthesis of thermoresistant engineering plastics.<sup>[20–22]</sup> However, aromatic biomolecule candidates with further potential need to be identified for use as renewable starting materials in novel biobased polymer synthesis.<sup>[23,24]</sup>

White biotechnological methods (i.e., combination of biotechnology and chemical engineering) enhance the production of bioderived precursors and are an important process for the diversification of the final products.<sup>[6]</sup> In a previous study, members of our group biotransformed 4-aminophenylalanine, which was produced using a genetically engineered bacterium, into 4-aminocinnamic acid (4ACA) by using a bacterium producing a phenylalanine ammonia lyase.<sup>[25]</sup> 4ACA was then photodimerized to produce the first biomass-derived aromatic diamine 4,4-diamino- $\alpha$ -truxillic dimethyl ester (4ATA ester). The resulting 4ATA ester was used as an aromatic building block for aromatic polymers such as polyureas, polyamides, and polyimides.<sup>[26–28]</sup> The thermal degradation temperatures of these three polymers (210, 273, and 425 °C, respectively) significantly exceed those of the conventional aliphatic bioplastics and partially resolved the issue of single usage. However, these values were significantly lower than those of petrochemical polybenzazoles whose thermal degradation temperatures vary between 600 and 700 °C.<sup>[29]</sup>

Since 1980, petrochemical polybenzazoles are considered to exhibit the best thermoresistance among organic materials due to their continuously resonating and repeating aromatic/heterocyclic structures.<sup>[30–32]</sup> Polybenzazoles are well-known not only for their excellent thermomechanical stability but also for their chemical resistance and radiation resistance as a result of extended conjugation and  $\pi$ - $\pi$  stacking structure.

Polybenzimidazoles (PBIs) are superior in terms of thermoresistance among polybenzazoles due to the presence of interchain hydrogen bonding (H-bonding).<sup>[33,34]</sup> Meanwhile, heavy inorganic fillers are conventionally used for increasing the thermoresistance temperature of organic materials.<sup>[35]</sup> However, it appears that no molecular designs have been proposed for some time, which is aimed at increasing the thermoresistance of organic plastics and simultaneously maintaining their light weight properties. The manufacturing of plastics without heavy or hard fillers of inorganics and/or metals has several advantages, including ease of manufacturing, reduced energy consumption, light-weight, and few processing steps.<sup>[36]</sup>

In this study we developed ultrahigh thermoresistance PBI films from inedible cellulose biomass and surpassed the upper limit of thermoresistant polybenzazoles. Due to their rigid aromatic backbones and  $\pi$ - $\pi$  stacking these biobased polymers outstand in terms of thermostability as compared with bioderived 4ATA based polyimides, polyureas, and polyamides.<sup>[26–28]</sup> The resonance stabilization energy was found to have a negative impact on interchain hydrogen bonds (H-bonds). The use of an inedible cellulosic feedstock to develop thermostable biobased plastics via novel molecular designing could achieve several of the SDGs, e.g., SDG 9 (industry, innovation, and infrastructure), SDG 2 (zero hunger), SDG 11 (sustainable cities and communities), and SDG 13 (climate action). The ultrahigh thermoresistant, light-weight bioplastics developed in this study are highly innovative; they can be used in the development of various high-performance products and has the potential to create a new industry. The use of inedible biomass avoids competition for food, which itself contributes to the eradication of hunger, as well as to a sustainable society that is not dependent on petroleum. The developed ultrahigh thermoresistant, light-weight bioplastics can be used as metal-alternatives for the engine and motor components of transportation equipment, including automobiles, watercraft, and aircraft, which would significantly improve their energy efficiency, facilitate the reduction of climate change, and contribute to creating a low-carbon society.

## 2. Results and Discussion

### 2.1. Designing and Preparation of Bioderived Monomers and Polymers

To develop bioderived PBI from fermentative products of cellulosic biomass, we first designed the molecular structures of PBI and its potential monomers. The benzimidazole bond responsible for the high thermostability is comprised of aromatic *ortho*-diamines and one carboxylic acid. The simplest PBI monomer is 3,4-diaminobenzoic acid (DABA); two DABA molecules can form a 2,5-benzimidazole bond (**Figure 1** and Scheme S1A, Supporting Information). Compared with another type of PBI, which is a polycondensation product of a di(*ortho*-diamino)aryl compound and an aromatic dicarboxylic acid (Scheme S1B, Supporting Information), poly(2,5-benzimidazole) (2,5-PBI) seems to be more suitable for biobased production due to its production via a simple polycondensation of only one monomer. Because no natural compound exists with the *ortho*-diaminobenzoic acid backbone, we searched for compounds

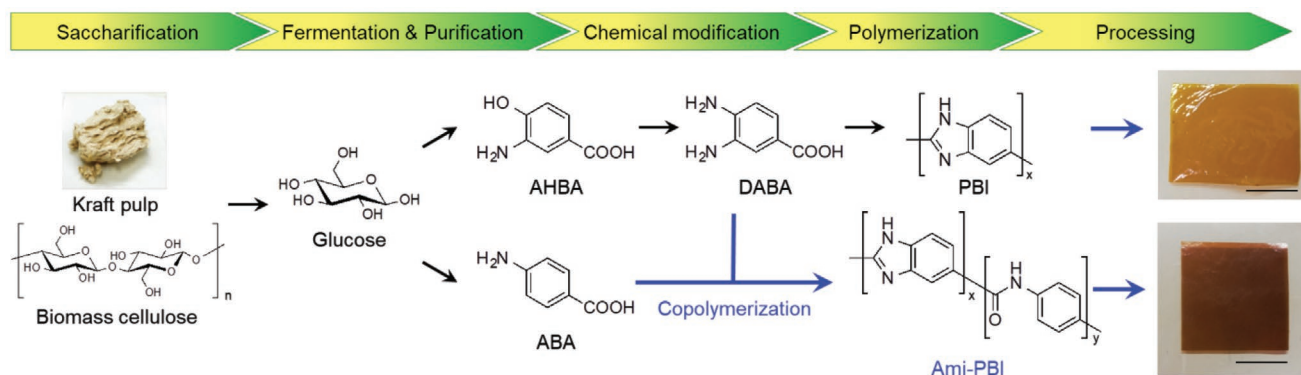


**Figure 1.** Production of PBI and Ami-PBI from cellulosic biomass. Kraft pulp (left) was enzymatically hydrolyzed (via saccharification). AHBA and ABA were produced from the kraft pulp hydrolysate using recombinant *C. glutamicum* and *E. coli* strains, respectively (via fermentation) and were highly purified before being subjected to subsequent chemical steps (via purification). AHBA was converted into DABA by the Smiles rearrangement (via chemical modification). DABA was polycondensed alone and copolycondensed with ABA to obtain PBI and Ami-PBI, respectively (via polymerization). Finally, PBI and Ami-PBI were cast into films (via processing; right pictures). Scale bar: 1 cm.

that can be i) converted to *ortho*-diaminobenzoic acid without employing complex chemical reactions and ii) produced in large amounts by a microorganism. Finally, we selected 3-amino-4-hydroxybenzoic acid (AHBA) as an ideal precursor of DABA (Figure 1 and Scheme S2, Supporting Information). Members of our group previously discovered two enzymes that facilitate the production of AHBA from the bacterium *Streptomyces griseus*<sup>[37]</sup> (Scheme S3, Supporting Information) and generated the recombinant *Corynebacterium glutamicum* strain KT01 for the production of AHBA.<sup>[38]</sup> The copolymerization of DABA with a small amount of a monoaminobenzoic acid introduces amide bonds into the PBI and may control its thermal performance.<sup>[39]</sup> We selected 4-aminobenzoic acid (ABA) as the comonomer. ABA is a monomer of a popular high-performance polyamide, *para*-aramid, and can be produced by recombinant bacteria capable of converting chorismate to ABA (Scheme S4, Supporting Information).<sup>[40,41]</sup>

We produced AHBA and ABA by fermentation, using kraft pulp as the starting material. Kraft pulp, which is recovered by fractionation processes in the paper industry, is an example of a model cellulosic feedstock, in addition to wood, energy crops, and agricultural residue.<sup>[42,43]</sup> In this study, kraft pulp was enzymatically hydrolyzed in an extremely low volume of reaction buffer to achieve a high glucose concentration in the hydrolysate. After 72 h of incubation, most of the kraft pulp liquefied yielding darkish-brown supernatant containing 60–80 g L<sup>-1</sup> glucose (Figure S1, Supporting Information). AHBA was then produced by the *C. glutamicum* strain KT01 in a mineral salt medium containing the kraft pulp hydrolysate as the sole carbon source (≈65% v/v, 377 g L<sup>-1</sup> glucose). In this medium, the cell growth (measured by the maximum optical density at 600 nm [OD<sub>600</sub>] after 192 h of incubation) decreased by 40%, but the AHBA production increased fourfold, compared to a control mineral salt medium containing authentic glucose (37 g L<sup>-1</sup>) (Figure S2, Supporting Information). The concentration of biomass-derived AHBA reached 3.1 ± 0.2 g L<sup>-1</sup> after 215 h of cultivation. The biobased AHBA was purified through a series of column chromatography and liquid–liquid extraction stages (Scheme S5 and Figure S3, Supporting Information) and was converted to DABA using the Smiles rearrangement

after simple chemical modifications that increased the nucleophilic reactivity of AHBA (Scheme S6, Supporting Information). We confirmed the chemical conversion of commercial (petroleum-derived) AHBA at each step by <sup>1</sup>H- and <sup>13</sup>C-NMR (Figures S4–S7, Supporting Information). The total yield of DABA hydrochloride was 17.6 mol% with a purity of over 99%. The ABA producer *Escherichia coli* HKE6054 expressing *pabABC* from *Pseudomonas protegens* was constructed and grown in a fermentation medium containing the kraft pulp hydrolysate (12% v/v, 75 g L<sup>-1</sup> glucose) for 48 h. ABA production was 0.81 ± 0.04 g L<sup>-1</sup> (yield = 14.2% mol mol<sup>-1</sup> vs glucose) (Figure S8, Supporting Information). Highly pure (>99%) hydrochloride salt of ABA (pale yellow powder) was precipitated in acetone after extracting the culture supernatant with ethyl acetate (Figure S9, Supporting Information).

We investigated the optimal conditions for the production of PBI polymers (DABA homopolymer, and copolymerizing DABA with ABA) using commercial AHBA-derived DABA and commercial ABA. Under the optimized conditions, Eaton's reagent (P<sub>2</sub>O<sub>5</sub>/methanesulfonic acid [1/10]) and poly(phosphoric acid) (PPA) were used as the condensation agents for the homopolymerization of DABA and its copolymerization with ABA, respectively, in various ratios to obtain the PBI-precursor polyamides (Schemes S7 and S8, Supporting Information). All of the PBI-precursor polyamides were heated to 400 °C to facilitate the dehydration of the amide with a contiguous amine to form an imidazole ring (Schemes S7 and S8, Supporting Information); brownish powders were obtained. The generation of benzimidazole bonds was confirmed by solid-state Fourier-transformed infrared (FT-IR); (Figures S10 and S11, Supporting Information) and <sup>13</sup>C-NMR spectroscopies (Figures S12 and S13, Supporting Information). The high inherent viscosity,  $\eta_{inh}$ , of the concentrated sulfuric acid solution for all of the PBI powders confirmed the high degree of polymerization (Table 1). All of the PBI polymers were less soluble in solvents than the corresponding precursor polyamides, but were solubilized with trifluoroacetic acid (TFA) containing 2–3% v/v methanesulfonic acid. Casting of the solubilized PBI polymers formed green/brown-colored films with moderate transparency (Figure 1, pictures on the right). Their X-ray diffraction (XRD) data

**Table 1.** Thermal and mechanical properties of PBI/Ami-PBI films, *para*-aramid, and other high-performance plastics.

Polymers <sup>a)</sup>	$\eta_{inh}^{b)}$ [dL g <sup>-1</sup> ]	$\rho^c)$ [g cm <sup>-3</sup> ]	$T_{d1}^{d)}$ [°C]	$T_{d10}^{d)}$ [°C]	CTE <sup>e)</sup> [°C]	Maximal stress <sup>f)</sup> [MPa]	Young's moduli <sup>f)</sup> [GPa]	Elongation at break <sup>f)</sup> [%]
2,5-PBI (DABA/ABA: 100/0)	2.3	1.35	475	700	18	75 ± 3.5	3.6 ± 0.5	2.6
Bio-2,5-PBI (100/0)	–	1.34	470	716	18	68	3.3	2.6
Ami-PBI (95/5)	2.4	1.36	495	720	19	71 ± 2.9	3.1 ± 0.7	3.1
Ami-PBI (90/10)	2.5	1.36	520	735	18	69 ± 3.4	3.1 ± 1.2	3.3
Ami-PBI (85/15)	2.6	1.38	575	745	19	68 ± 1.7	3.2 ± 0.3	3.4
Bio-Ami-PBI (85/15)	–	1.36	580	743	19	66	3.2	3.0
Ami-PBI (80/20)	2.4	1.39	440	697	19	63 ± 2.4	2.8 ± 0.9	3.6
Ami-PBI (60/40)	2.2	1.39	435	683	24	52 ± 2.7	2.1 ± 0.6	3.8
Ami-PBI (50/50)	2.1	1.39	430	640	32	42 ± 3.2	1.8 ± 1.1	4.7
<i>para</i> -Aramid (0/100)	1.9	1.41	370	485	–	33 ± 1.4	1.4 ± 0.2	5.5
Zylon	–	1.56	565	715	–6	5800	180	3.5
Kevlar 49	–	1.44	275	585	8.3	300	112	2.4
Kapton	–	1.42	500	580	32	231	2.5	72
Celazole	–	1.30	165	570	23	100	5	2.2
PEEK	–	1.32	525	570	55	98	4	45
PPS	–	1.44	495	530	50	93	3.5	15
Nylon 6	–	1.14	390	415	80	75	2.4	15

<sup>a)</sup>Seven conventional high-performance plastics are presented for comparison: polybenzoxazole (PBO) Zylon,<sup>[30]</sup> *para*-aramid (PA) Kevlar 49,<sup>[44]</sup> polyimide (PI) Kapton,<sup>[45]</sup> PBI Celazole,<sup>[31,32]</sup> polyetheretherketone (PEEK),<sup>[46,47]</sup> polyphenylenesulfide (PPS),<sup>[48]</sup> and poly( $\epsilon$ -caprolactam) Nylon 6;<sup>[49,50]</sup> <sup>b)</sup>Inherent viscosity of concentrated sulfuric acid solution of each PBI polymer; <sup>c)</sup>Density of the polymer samples in water at room temperature; <sup>d)</sup>Determined by thermogravimetry under a nitrogen atmosphere; <sup>e)</sup>Coefficient of thermal expansion (CTE) was measured using thermomechanical analysis (TMA) under a load of 3.0 g and heating rate of 2 °C min<sup>-1</sup>; <sup>f)</sup>Obtained from stress–strain curves in elongation mode.

indicated that the PBI polymers were partially crystallized and that their crystallinity decreased as the ABA fraction increased (Figure S14, Supporting Information). It is worth noting that the ABA homopolymer, *para*-aramid, is an amorphous polymer.

## 2.2. Thermal Property Analysis

The effects of incorporating ABA into PBI on the thermal and mechanical properties of the resulting PBI films were investigated in detail. We designated the copolymer of DABA with ABA as amide-containing PBI (Ami-PBI). The thermal degradation behavior of the PBI films was investigated by

thermogravimetric analysis (TGA) under a nitrogen atmosphere (Figure 2). A mass loss was observed for the PBI films at >430 °C and at >370 °C for the aramid (Figure 2A). In Figure 2B, the temperatures at which mass losses of 1% and 10% ( $T_{d1}$  and  $T_{d10}$ , respectively) were observed under pyrolysis conditions (Table 1) are plotted against the ABA content in PBI. The temperatures at which mass losses of 1% and 10% ( $T_{d1}$  and  $T_{d10}$ , respectively) were observed under pyrolysis conditions (Table 1) are plotted against the ABA content in PBI (Figure 2B). The  $T_{d10}$  values for the Ami-PBI films ranged from 640 to 745 °C with the maximum value obtained for Ami-PBI of 15 mol% ABA. The  $T_{d1}$  values for the Ami-PBI films ranged from 430 to 575 °C, which is considerably higher than those

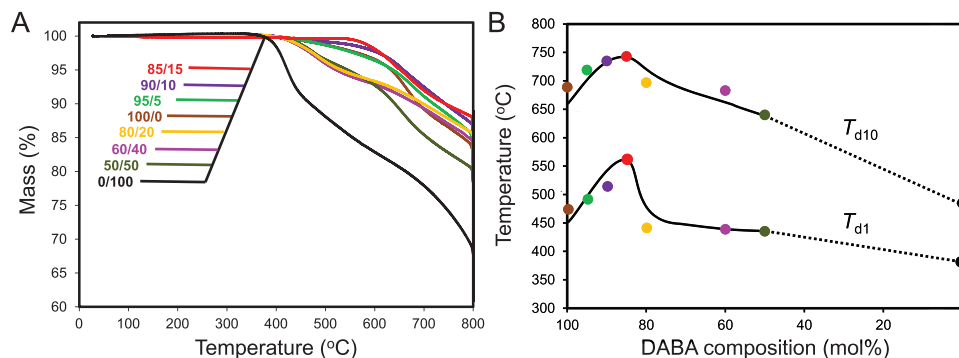


**Figure 2.** Thermal properties of PBI and Ami-PBI films. a) TGA curves recorded under a nitrogen atmosphere. The molar ratio of DABA/ABA of each polymer film is shown; 100/0 and 0/100 represent 2,5-PBI (homopolymer of DABA) and *para*-aramid (homopolymer of ABA), respectively. b) The 1% and 10% mass-loss temperatures ( $T_{d1}$  and  $T_{d10}$ , respectively) of each polymer film are plotted against its DABA composition.

of most conventional high-performance plastics (Table 1). The  $T_{d10}$  and  $T_{d1}$  values for the PBI films in air ( $>495$  and  $>420$  °C, respectively) were also high and varied depending on the ABA content (Figures S15 and S16 and Table S1, Supporting Information). The Ami-PBI of 15 mol% ABA showed the highest values ( $T_{d10}$ , 690 °C;  $T_{d1}$ , 495 °C). While the ABA homopolymer is less thermostable than PBI, incorporating relatively small amounts of ABA into the PBI backbone increased the thermal stability of the resulting Ami-PBI films. This unique thermal stability may be explained by interchain H-bonds in amorphous regions as described below.

In spite of strengthened H-bonding, the densities ( $\rho$ ) of the Ami-PBI polymer films (1.36–1.39 g cm<sup>-3</sup>) were lower than other rigid chain polymers for ultrahigh-performance plastics (Table 1) due to the asymmetric structures along and across the polymer chain axes. A perfect balance between lightweight and ultrahigh thermoresistance can make Ami-PBI a strong candidate for various applications in the development of a sustainable society. It can be used in the manufacturing of internal combustion engine components (e.g., seals, bearings, and insulation bushings), heat-resistant panels, gaskets, compressor seals in jet engines, and automobile exhaust systems.<sup>[51,52]</sup>

The combustion behavior of a representative Ami-PBI film (15 mol% ABA) was examined (Movie S1, Supporting Information). The Ami-PBI film showed excellent properties suitable for use in ultrahigh thermoresistant materials, including very strong self-extinguishment and no drip during combustion (UL-94 V-0 rating).<sup>[53]</sup> The char yields for Ami-PBI of 15 mol% ABA at 800 °C were 89% under nitrogen and 84% under air, which were much higher than those of conventional fully aromatic polymers with high flame retardance (Kapton, 53%;<sup>[45]</sup> poly(*p*-phenylenebenzobisoxazole), 61%;<sup>[30]</sup> both under nitrogen).

### 2.3. Theoretical Calculation

The imidazole N–H groups of canonical PBI are able to bind with the  $-N=$  groups of the adjacent PBI chains via H-bonds (Figure 3). The incorporation of amide bonds into PBI can introduce new H-bonds of amide–imidazole and amide–amide around the amide linkage. To compare the H-bond energies of imidazole–imidazole, amide–imidazole, and amide–amide, density functional theory (DFT) calculations were performed using low-molecular-weight models: 2-phenylbenzimidazole

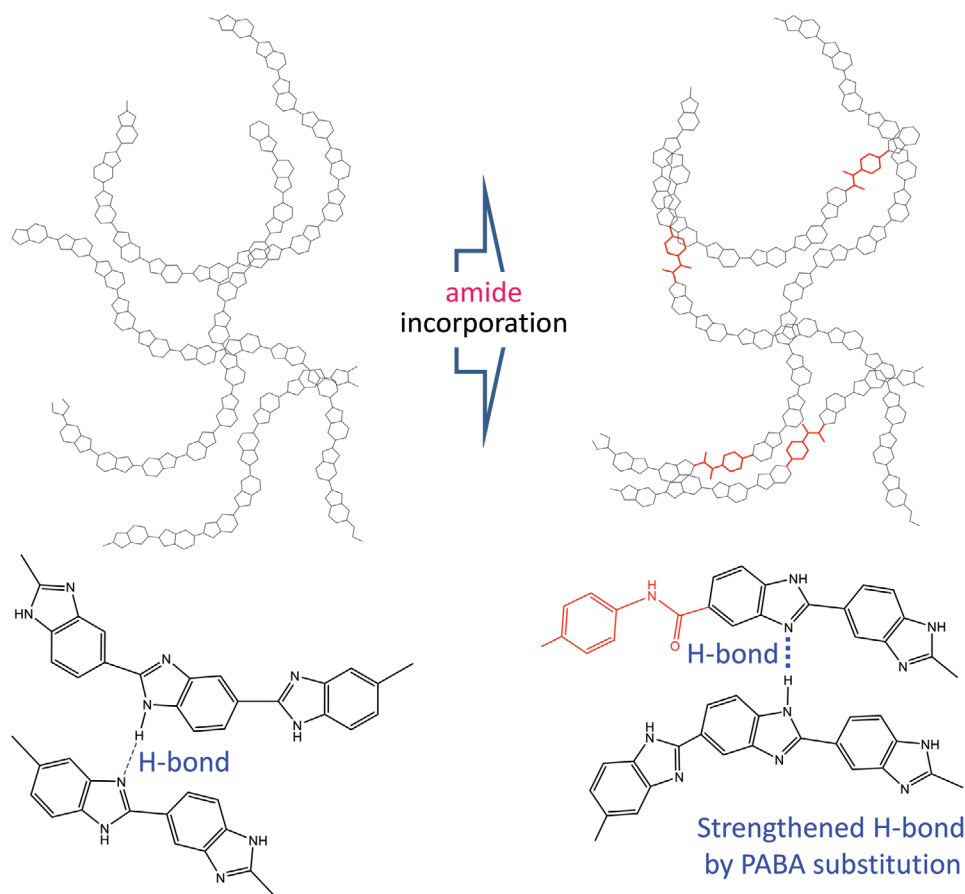


**Figure 3.** Schematic illustration of possible H-bonds between 2,5-PBI polymer chains (left) and between Ami-PBI polymer chains (right) in amorphous regions. Interchain hydrogen bonds (dotted line) can form between the H atom of N–H and the  $-N=$  atom of two adjacent imidazole rings. As a result of DFT calculation, the hydrogen bond (indicated by a thick dotted line) formed between two adjacent imidazole rings near the amide linkage, i.e., near the ABA-derived portion (red), was strengthened as a result of the reduced R-effect.

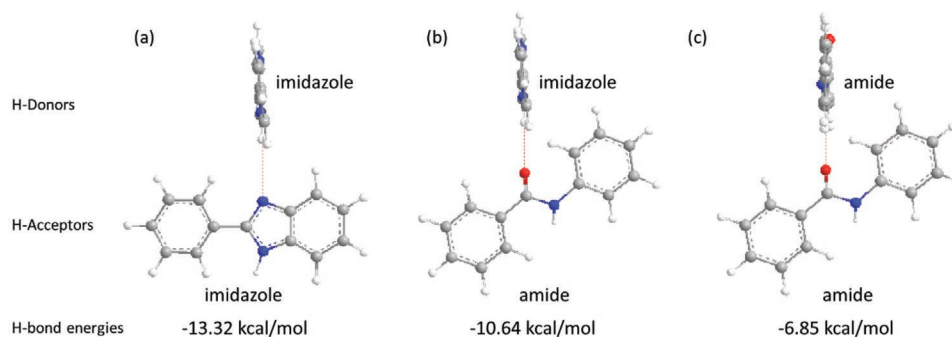


**Figure 4.** Hydrogen bonding energy of geometrically optimized molecular models. Values calculated using the DFT method are shown below the structures of a) imidazole (N–H)/imidazole (C=N), b) imidazole (N–H)/amide (C=O), and c) amide (N–H)/amide (C=O).

(2BI) for the benzimidazole portion and benzanilide (BA) for the ABA-derived portion. Two models were used to study the interaction between N–H of 2BI or BA (H-donor) and –N= of 2BI or O=C of BA (H-acceptor) arranged orthogonally (Figure 4) to minimize the unexpected interactions between both models. H-bond energies between two 2BI models (Figure 4a), 2BI and BA models (Figure 4b), and two BA models (Figure 4c) were calculated as  $-13.32$ ,  $-10.64$ , and  $-6.85$  kcal mol $^{-1}$ , respectively. Namely, the H-bond between the two imidazole rings was the strongest among the three H-bond interactions. As a result, a high thermal degradation temperature of PBI could be attributed to strong H-bonds between two imidazole rings and that the weaker H-bond interactions of imidazole–amide and amide–amide reduced the thermal degradation temperatures of Ami-PBIs with high ABA incorporation (>20%).

To determine the underlying mechanism for the increased thermal degradation temperatures of Ami-PBIs with low ABA incorporation (<20%), the influence of amide linkage on the

H-bond energy between two imidazole rings (one located next to the amide linkage) was estimated with the DFT calculation using a combination of three lengthened PBI and Ami-PBI models: i) 2-phenyl(2,5-terbenzimidazole) (BI-BI-BI), ii) 5'-benzamide-2'-(2-phenylbenzimidazole)benzimidazole (BA-BI-BI), and iii) 2'-(4-benzamidephenyl)-2,5'-bibenzimidazole (BI-BI-BA) (Figure 5). These three models were used to study the interaction between the imidazole N–H (H-donor) and imidazole –N= (H-acceptor) of each central BI unit, and they were orthogonally arranged in a manner similar to that shown in Figure 4a. The H-bond energy between the two BI-BI-BI models was estimated as  $-4.77$  kcal mol $^{-1}$ . Meanwhile, the H-bond energies between BI-BI-BI (H-donor) and BA-BI-BI (H-acceptor) and between BA-BI-BI (H-donor) and BI-BI-BI (H-acceptor) were calculated as  $-10.01$  and  $-10.58$  kcal mol $^{-1}$ , respectively. Similarly, the H-bond energies between BI-BI-BI (H-donor and H-acceptor) and BI-BI-BA (H-acceptor and H-donor) were estimated as  $-12.68$  and  $-12.46$  kcal mol $^{-1}$ , respectively. Therefore,

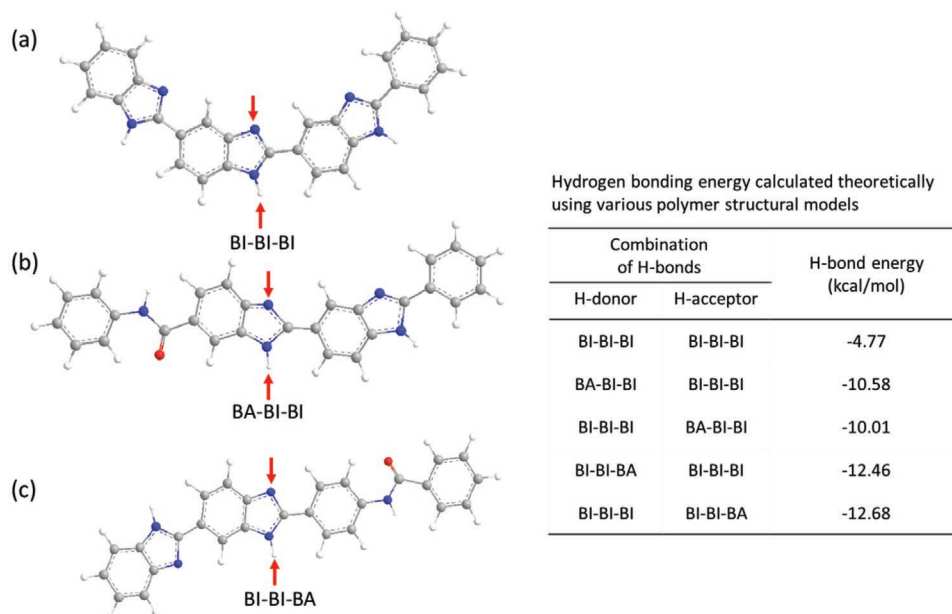


**Figure 5.** Structures of geometrically optimized molecular models for a) PBI and b,c) Ami-PBI. a) 2-Phenyl(2,5-terbenzimidazole) [BI-BI-BI], b) 5'-benzamide-2'-(2-phenylbenzimidazole)benzimidazole [BA-BI-BI], and c) 2'-(4-benzamidephenyl)-2,5'-bibenzimidazole [BI-BI-BA] were used for calculating the H-bonding energy between two imidazoles. The central imidazoles (arrows) were targeted. The table shows information on the H-bonding energy for various combinations of these models.

the absolute values of the H-bond energies between the PBI model and either of the two Ami-PBI models were much higher than the absolute value of the H-bond energy between the two PBI models. This indicates that the incorporation of a small amount of ABA units into PBI chains enhanced the strength of the interchain H-bond between two imidazole rings (one of which locates next to the resulting amide bond), increasing the thermal resistance temperatures.

This result can be discussed in terms of the inductive (I) and resonance (R) effects of the amide group on the adjacent imidazole ring. The I-effect should induce contrasting effects on both the H-donor of N–H and the H-acceptor of –N= on the central imidazole. Therefore, the I-effect should not affect the H-bond energy significantly. However, the R-effect should be significant for the H-bond energy, since the absolute value of the H-bond energy between the central imidazoles of the two BI-BI-BI models ( $-4.77 \text{ kcal mol}^{-1}$ ) was markedly reduced compared to the 2BI models ( $-13.32 \text{ kcal mol}^{-1}$ ) (Figure 4a). This indicates that the enhancement of the intrachain resonance of the imidazole ring should weaken the interchain H-bond. In both BA-BI-BI and BI-BI-BA, the substitution of a BA unit for a terminal BI unit appeared to reduce the R-effect and strengthen the H-bond energy between the central imidazoles. Previously reported poly(PBO-co-PBI)s, synthesized via the copolymerization of AHBA with DABA, where polybenzoxazole (PBO) incorporation had a strong R-effect on the PBI chains to reduce the H-bond energy between interchain imidazoles, resulted in a monotonous decrease in  $T_{d10}$  from 716 to 622 °C, with an increasing PBO composition.<sup>[54]</sup> This supports our results, in which the H-bonding energy was found to increase after the incorporation of ABA to PBIs.

#### 2.4. Mechanical Property Analysis

The linear thermal expansion coefficient (coefficient of thermal expansion, CTE) of the polymers was analyzed by thermo-mechanical analysis (TMA) (Table 1). The CTE values of the homopolymer PBI and copolymers Ami-PBI with low ABA incorporation ( $\leq 20\%$ ) were 17–20 ppm  $\text{K}^{-1}$ . As the amount of ABA incorporated increased, the CTE values of Ami-PBI increased. These low CTE values ( $\approx 20.0 \text{ ppm K}^{-1}$ ) are comparable to those of certain metals including aluminum, copper, and silver and are very significant for future research on the development of metal-substitute materials for use in engine rooms.<sup>[55,56]</sup> Heat distortion was not detected below degradation temperatures.

The tensile stress–strain properties of the PBI films were also analyzed (Table 1 and Figure S17, Supporting Information). The DABA homopolymer film showed the highest tensile strength (75 MPa) and Young's modulus (3.6 GPa) of all of the PBI films produced in this study. The tensile strength and Young's modulus values of Ami-PBI films ranged from 73 to 42 MPa and 3.4 to 1.8 GPa, respectively, both of which decreased as the ABA content increased. The DABA homopolymer film showed the lowest value for tensile elongation at break (2.6%). These values gradually increased as the ABA composition increased up to 5.5%. These results suggest that the highly rigid structure of PBI was responsible for the high mechanical strength

and low value of tensile elongation at break. Most of the PBI films produced in this study showed higher tensile strength values than those of conventional aliphatic bioplastics, such as poly(butylenesuccinate) (34 MPa), poly(3-hydroxybutyrate) (40 MPa), PLA (60 MPa), and they were comparable with those of the available aromatic bioplastics such as polyimide, polyesters.<sup>[57–60]</sup> The processability of PBI into films is very important for its application in manufacturing, from plastics or matrices to composites with metals with high melting temperatures. The molecular rigidity of the fibrous materials of conventional high-performance polymers is too high for their processing into films.

#### 2.5. Comparing Bioderived and Commercially Derived Polymer Performance

Lastly, we produced two biobased PBI films of 2,5-PBI and a representative Ami-PBI (15 mol% ABA) from kraft pulp-derived compounds (AHBA for both, ABA for the Ami-PBI). Both cellulose-derived PBI films showed comparable thermal and mechanical properties to those of corresponding polymer films produced from the commercially available compound(s) (Table 1 and Figures S18 and S19, Supporting Information).

### 3. Conclusion

In this study, we designed a novel structure of sustainable polymers to address the challenges and opportunities currently faced in the use and manufacturing of bioplastics. Genetically engineered bacterial strains were generated for the production of two aminobenzoic acid monomers from a renewable cellulosic feedstock, and high-performance PBI bioplastic films were produced. We proposed that incorporation of a small amount of ABA strengthens the interchain H-bonding of the novel PBI bioplastics; the resulting biobased Ami-PBI of 15 mol% ABA showed a higher thermoresistance ( $T_{d10}$ : 743 °C) than any currently existing biomass- or petroleum-derived plastics, including polybenzazoles, which have been considered the ideal thermoresistant plastic for around 40 years. Thus, we have succeeded in breaking the upper limit of the thermoresistance of plastics and the thermoresistance of the newly developed PBIs is in the same range as that of inorganics. As a future perspective, such a high thermoresistance and good processability would enable the plastics to be hybridized with metals and/or inorganic compounds at a temperature above their melting points without thermally degrading the contacting plastics. Ami-PBI showed a high thermoresistance while maintaining a lower density than most of the conventional high-performance plastics, including Kevlar, Kapton, and Zylon, among others. Considering glass-fiber-reinforced polyphenylenesulfide (density:  $1.66 \text{ g cm}^{-3}$ ) and liquid crystalline polymers (density:  $1.61 \text{ g cm}^{-3}$ ), the ultrahigh thermoresistance and lightweight of Ami-PBI (density:  $1.36 \text{ g cm}^{-3}$ ) means it could be used in the manufacture of engine components to improve energy efficiency for hybrid electric vehicles sensitive to weight. Moreover, PBI bioplastics could be inserted as high-thermoresistance insulators between conducting metals to create high-performance

electronic devices, including super-integrated circuits, mass memories, and high-power motors, opening the door to a new scientific era of lightweight materials and a more sustainable society.

## 4. Experimental Section

Detailed experimental methods can be found in the Appendix of the Supporting Information.

**Enzymatic Hydrolysis of Kraft Pulp:** Laubholz unbleached Kraft pulp (LUKP) was kindly supplied by Nippon Paper Group (Tokyo, Japan). The component ratios of glucan and xylan in the LUKP were 71.0% and 22.4%, respectively.<sup>[62]</sup> Enzymatic saccharification of the LUKP was performed in a 2 L jar fermenter (DPC-3A) equipped with a MaxBlend impeller (ABLE Co. and Biott Co., Ltd, Tokyo, Japan) using a cellulose enzyme blend (Sigma-Aldrich Co. limited liability company, St. Louis, MO) containing 440 g of wet LUKP (65% water content; corresponding to 154 g dry weight biomass) and 1050 mL of sodium citrate buffer ( $50 \times 10^{-3}$  M, pH 4.8). The wet LUKP was initially kneaded by rotating at 160 rpm for 90 min at 50 °C. A cellulase enzyme blend was added into the premixture at an enzyme load of 5 filter paper units (FPU)  $g^{-1}$  dry biomass and enzymatic hydrolysis was conducted for 72 h at 50 °C. After saccharification, the residual solids were removed from the resulting hydrolysate and the supernatant was collected by centrifugation ( $9000 \times g$  for 15 min at 4 °C). The supernatant was aseptically filtrated using the membrane filter Rapid-Flow (Thermo Fisher Scientific, Waltham, MA, USA). The resulting filtrate, designated as kraft pulp hydrolysate, was stored at -30 °C.

**Fermentative Production of AHBA from Kraft Pulp Hydrolysate:** A recombinant *C. glutamicum* strain KT01, containing *grtH* and *grtI* derived from *S. griseus*,<sup>[8,9]</sup> was precultured aerobically until late log phase in 10 mL of Brain Heart Infusion broth (Becton, Dickinson and Company, Franklin Lakes, NJ, USA) in a 50 mL test tube with constant agitation (180 rpm) for 18 h at 26 °C. The preculture was transferred to 750 mL of CGXII medium<sup>[61]</sup> (supplemented with 100 mg  $L^{-1}$  of leucine and 100 mg  $L^{-1}$  of pantothenate) containing kraft pulp hydrolysate ( $\approx 65\%$  v/v, 37.7 g  $L^{-1}$  glucose) in a 2 L jar fermenter (BMZ-02KP2, ABLE Co. and Biott Co.) to obtain a cell concentration corresponding to an optical density at 600 nm ( $OD_{600}$ ) of 0.2 in Brain Heart Infusion broth. The cultivation conditions were as follows: temperature, 26 °C; pH, 7.0 (maintained by the addition of ammonia); stirrer speed, 190 rpm; aeration with compressed air, 0.5 vvm.

**Purification of AHBA from Fermentation Broth:** Scheme S5 in the Supporting Information shows the total process of AHBA purification. AHBA was purified from fermentation broth (Figure S3, Supporting Information) by column chromatography using PoraPak Rxn CX (Waters, Milford, MA, USA), silica gel column chromatography (Silica gel 60, 0.040–0.063 mm, [Merck] Darmstadt, Germany), octadecylsilyl column chromatography (COSMOSIL 75C<sub>18</sub>-OPN, Nacalai Tesque, Kyoto, Japan), and partition between ethyl acetate and H<sub>2</sub>O, as described in the Supporting Information. The average yield of AHBA was 41%.

**Analytical Procedures in AHBA Fermentation and Purification:** Culture samples or chromatography fractions were centrifuged ( $15\,000 \times g$  for 10 min at 4 °C) and the concentrations of glucose, AHBA, organic acids, and amino acids in each supernatant were measured. The concentrations of AHBA and organic acids were determined by high-performance liquid chromatography, as described previously.<sup>[9]</sup> Cell mass was estimated by measuring  $OD_{600}$  using a spectrophotometer (U-3010; Hitachi, Tokyo, Japan). The concentrations of the target compounds were calculated based on standard curves obtained using authentic samples.

**Production of ABA from Kraft Pulp Hydrolysate:** Strains, primers, and plasmids are listed in Table S2 in the Supporting Information. As described in the Supporting Information, several recombinant *E. coli* strains for the production of ABA were generated. Ultimately, the best producer, *E. coli* HKE6054 expressing *pppabABC*, was selected.

This strain was grown in a fermentation medium containing kraft pulp hydrolysate of a final concentration of 7.5 g  $L^{-1}$  glucose. Triplicate cultures (500 mL each) produced  $\approx 2.4$  g cellulose-derived ABA. The culture supernatant was collected by centrifugation ( $5000 \times g$  for 20 min at 4 °C), adjusted to pH 3.0 by HCl, and extracted with an equal volume of ethyl acetate. After the organic layer was evaporated, the resulting dark yellow powder was dissolved in acetone, and the ABA-HCl salt was precipitated by adding HCl. The precipitate was collected by filtration on Advantec filter paper No. 2 (Toyo Roshi Kaisha, Tokyo, Japan) and rinsed with 0.1% HCl in acetone to obtain 1.5 g of  $>99\%$  pure pale yellow product (Figure S9, Supporting Information).

**Materials for Chemical Experiments:** Commercial AHBA, ABA, and DABA were purchased from Tokyo Chemical Industry (TCI) (Tokyo, Japan). For monomer synthesis, 2-bromoisobutylamide and potassium peroxydisulfate were purchased from TCI, and potassium carbonate ( $K_2CO_3$ ), potassium hydroxide (KOH), hydrochloric acid (HCl), methanesulfonic acid ( $MeSO_3H$ ), phosphorus pentoxide ( $P_2O_5$ ), and conc. sulfuric acid ( $H_2SO_4$ ) were purchased from Kanto Chemicals Co. Ltd. (Tokyo, Japan). Methanol, acetone, hexane, TFA, *N,N*-dimethylacetamide (DMAc), dimethylsulfoxide (DMSO), dichloromethane, and DMSO-*d*<sub>6</sub> (NMR solvent) were purchased from Kanto chemicals Co. Ltd. and were used as solvents without purification. Palladium-charcoal (5%) purchased from Sigma-Aldrich was used as a catalyst of hydrogen reduction. Eaton's reagent ( $P_2O_5$ /methanesulfonic acid 1/10) and PPA were purchased from TCI, for use as polymerization solvents.

**Monomer Synthesis:** DABA was synthesized from bioderived AHBA as shown in Scheme S6 in the Supporting Information. Briefly, the amine group in bioderived AHBA was oxidized to prepare 4-hydroxy-3-nitrobenzoic acid followed by methyl esterification of the -COOH group to establish a site selective Smiles rearrangement, resulting in 4-hydroxy-3-nitrobenzoic acid methyl ester. The Smiles rearrangement reaction was performed to change hydroxyl (OH) into amine (-NH<sub>2</sub>) thereby obtaining 4-amino-3-nitrobenzoic acid. In the final step the nitro group (-NO<sub>2</sub>) was reduced simultaneously with -COOMe to obtain DABA. The steps in this process and the structural characterizations are described in more detail in the Supporting Information.

**Polymer Synthesis and Film Casting:** The PBIs were synthesized by the thermal cyclization reaction of the precursor polyamides with an amine group contiguous to each amide linkage. TGA under nitrogen examining the homopolymer of DABA and copolymers of DABA with ABA (DABA:ABA = 90:10, 85:15, and 80:20) was used to determine their thermal ring closing temperatures. At temperatures ranging from 390 to 410 °C, the masses of all the PBI and Ami-PBI precursors decreased by 8.1–11.7%, which was roughly in agreement with the theoretical mass loss after the elimination of one H<sub>2</sub>O molecule per amide with a contiguous amine (e.g., 13.4% for the homopolymer of DABA and 11.0% for the copolymer with 20 mol% ABA). This indicated that the amide with a contiguous amine was cyclized around these temperatures (Figure S20, Supporting Information). Based on these results, 400 °C was selected for the thermal cyclization temperature for 2,5-PBI and all Ami-PBIs.

**Synthesis of Homopolymer of DABA, Poly(2,5-benzimidazole) (2,5-PBI):** DABA·2HCl (0.58 g, 2.6 mmol) and  $P_2O_5$  (0.51 g, 3.6 mmol) were purged with nitrogen gas in a 30 mL round-bottomed flask. Then,  $MeSO_3H$  (4 mL) was added as the solvent using a syringe and the polymerization mixture was stirred for 24 h at 150 °C. The resulting mixture was poured into pure water (100 mL) to form a spherical precipitate of the polyamide precursor of PBI, which was dried at 110 °C under vacuum. The resulting solids were ground into a powder using a mortar-mill and washed with pure water. After drying under vacuum at 100 °C, the powder was heated stepwise at 100, 200, 300, and 400 °C (1 h at each temperature) under nitrogen to obtain poly(2,5-benzimidazole) (2,5-PBI; 0.23 g, 76.2%) (Scheme S7, Supporting Information).

**Synthesis of Copolymer of DABA and ABA, Poly(DABA-co-ABA) (Ami-PBI):** For the synthesis of a representative copolymer Ami-PBI of 15 mol% ABA, PPA (30 g) was placed in a three-necked round-bottom flask and dried at 120 °C for 1 h under N<sub>2</sub> flow. DABA·2HCl (1.887 g, 8.5 mmol) and ABA-HCl (0.237 g, 1.5 mmol) were mixed and added



carefully into the flask maintaining N<sub>2</sub> atmosphere. The reaction mixture was stepwise heated to 120 °C (1 h), 160 °C (4 h), and 220 °C (16 h) to complete the polymerization under N<sub>2</sub> flow. The resulting viscous brown liquid was precipitated in 200 mL of water, resulting in the formation of a polyamide precursor of Ami-PBI, in the form of a sticky rubber-like liquid. This liquid was solidified by drying at 110 °C for 4 h before crushing into a powder. The powder of the polyamide precursor of Ami-PBI still included a small amount of PPA and was washed with KOH aqueous solution (10%) and deionized water repeatedly until the pH of the cleaning liquid became 7 (checked with a pH test paper; Macherey-Nagel GmbH & Co. KG, Düren, Germany). The washed powder was dried at 100 °C under vacuum to obtain the polyamide precursor of Ami-PBI. The precursor powder was thermally treated by stepwise heating at 100, 200, 300, and 400 °C (1 h at each temperature) under N<sub>2</sub> atmosphere. The structure of the resulting powder substance was confirmed to be Ami-PBI by FT-IR and solid-state NMR spectroscopies. All other Ami-PBIs were obtained by the same method (Scheme S8, Supporting Information).

**Film Casting:** PBI powder was dissolved in the TFA and CH<sub>3</sub>SO<sub>3</sub>H (2–3%) mixture to obtain a 15 wt% solution in a flask. Nitrogen was bubbled into the closed flask to expel oxygen from the solution. The solution was heated and maintained at 65 °C for 15–18 h for homogenization. Any remaining solids were removed by filtration. The resulting homogeneous solution was cast over a glass substrate to make obtain a film. The film was peeled from the glass substrate and dipped in KOH aqueous solution (10%) for 12 h, followed by drying under vacuum, with the temperature increasing at a rate of 0.8–1.0 °C min<sup>-1</sup> to 200 °C, then maintained at 200 °C for 15 h to remove the residual solvents. After cooling spontaneously, a tough brown film was obtained. The Ami-PBI film was created using the same procedure.

**Characterization Methods:** High-resolution NMR spectra (<sup>1</sup>H at 400 MHz and <sup>13</sup>C at 100 MHz) in DMSO-*d*<sub>6</sub> were obtained on a Bruker NMR spectrometer model AVANCE III 400 with broadband fluorine observe smart probe plus automatic tuning and matching accessory probe operating at 400.13 MHz. <sup>13</sup>C solid-state NMR was run at 500 MHz on a Bruker Avance III spectrometer at a spinning speed of 8 kHz using a standard crosspolarization pulse sequence for cross polarization total sideband suppression or at a spinning speed of 4 kHz using the dipolar decoupled-magic angle spinning method.

The samples were packed in a 7 mm diameter zirconia rotor with a Kel-F cap and were spun at 10 kHz with a contact time of 2 ms and a period between successive accumulations of 5 s. The total number of scans was 10 000. Fourier transformed infrared spectra (FT-IR) were recorded on the PerkinElmer Spectrum One spectrometer using a diamond-attenuated total reflection accessory. TGA was conducted using a Hitachi STA7200. Briefly, the samples (<5 mg) were placed in a platinum crucible and heated to the maximum temperature of 800 °C at a rate of 5 °C min<sup>-1</sup> in an air and nitrogen atmosphere. The residual polymer yield (char yield) was determined, with the temperatures at the starting of degradation (*T*<sub>onset</sub>), 1% mass loss (*T*<sub>d1</sub>), and 10% mass loss (*T*<sub>d10</sub>). TMA was carried out using HITACHI TMA7100C (tensile mode) under nitrogen flow (flow rate, 200 mL min<sup>-1</sup>) from 50 to 500 °C with a heating rate of 2 °C min<sup>-1</sup> and a fixed load of 3.0 g to determine the CTE of the obtained polymers. Stress–strain analysis of the films prepared over a 10 mm length was performed in the elongation mode with a crosshead speed of 1 mm s<sup>-1</sup> at room temperature using a tensile testing machine (3365-L5, INSTRON) with a load cell (5 kN). The stress–strain curves of the five specimens were averaged to obtain the mean values for Young's moduli (*E*), tensile strength ( $\sigma$ ), and elongation at break ( $\epsilon$ ). The crystalline property was analyzed by powder XRD using a Rigaku Smartlab instrument at 40 kV, 200 mA, and a rate of 1° min<sup>-1</sup> using monochromated Cu K $\alpha$  radiation ( $\lambda$  = 0.15418 nm). The degree of crystallinity was quantitatively estimated according to the method described by Nara and Komiya.<sup>[63]</sup> The inherent viscosity of the polymers (0.5 g dL<sup>-1</sup>) in concentrated sulfuric acid solution was measured at 30 °C using a Ubbelohde viscometer (Sibata Scientific Technology Ltd.).

**Theoretical Calculation Method:** The H-bond interactions between imidazole N–H (H-donor) and H-acceptors such as –N= of imidazole

and C=O of amide in the homopolymer PBI and different copolymers were estimated as the standard energy difference between the donor and acceptor.<sup>[64]</sup> The representative donor and the acceptor unit structures were energy minimized separately by geometry optimization and brought into close contact in a complex structure using the same distance. To simplify the calculation process, a uniform intermolecular distance (about 3 Å) for H-bond interaction (between donor N–H and acceptor –N= or C=O) was used.<sup>[64]</sup> Neighboring atom interactions were avoided by orthogonally orienting the donor and acceptor molecular units.

All of the DFT simulations were performed using *Gaussian 16*, with the same basis set and structural orientation. The hybrid exchange-correlation function of Coulombic attenuating method<sup>[65]</sup> with conventional B3LYP (Becke, three-parameter LYP correlation function of Lee, Yang, and Parr) was introduced for a long-range correction as proposed by Tawada et al.<sup>[66]</sup> The basis set, cc-pVQZ (cc-p: correlation-consistent polarized, V: valance only basis set, QZ: quadruple-zeta), was used by the electronic orbital wave functions to optimize the geometry of the H-bond complexes.<sup>[67]</sup> Counterpoise correction was further employed in each case during geometry optimization and energy calculation to minimize basis-set superposition error.<sup>[68]</sup>

## Supporting Information

Supporting Information is available from the Wiley Online Library or from the author.

## Acknowledgements

The authors thank Dr. Akira Isogai for thoughtful encouragement in the Core Research for Evolutional Science and Technology (CREST) program. This work was supported by Japan Science and Technology Agency (CREST, Grant No. JPMJCR13B3 to Y.O., T.K., C.O., and N.T.). This work was also supported in part by the Cabinet Office, Government of Japan, Cross-ministerial Strategic Innovation Promotion Program (SIP), “Technologies for Smart Bio-industry and Agriculture” (funding agency: Bio-oriented Technology Research Advancement Institution, NARO, Grant No. 18087978 to Y.O., T.K., and N.T.) and Japan Society for the Promotion of Science (A3 Foresight Program to Y.O.). The authors are grateful to Prof. Kenta Hongo and Ken Sinkou Qin in Energy and Environment area, JAIST for their suggestions regarding theoretical calculations.

## Conflict of Interest

The authors declare no conflict of interest.

## Keywords

bioplastics, cellulose, density functional theory, high performance polymers, polybenzimidazole

Received: August 17, 2020

Revised: September 7, 2020

Published online: October 13, 2020

[1] D. Griggs, M. Stafford-Smith, O. Gaffney, J. Rockström, M. C. Öhman, P. Shyamsundar, W. Steffen, G. Glaser, N. Kanie, I. Noble, *Nature* **2013**, 495, 305.

[2] EUBIO Admin. (n.d.), European Bioplastics, <https://www.european-bioplastics.org/market/> (accessed: February 2020).

- [3] N. Peelman, P. Ragaert, K. Ragaert, B. D. Meulenaer, F. Devlieghere, L. Cardon, *J. Appl. Polym. Sci.* **2015**, *132*, n/a.
- [4] R. P. Babu, K. O'Connor, R. Seeram, *Prog. Biomater.* **2013**, *2*, 8.
- [5] H. Kawaguchi, C. Ogino, A. Kondo, *Bioresour. Technol.* **2017**, *245*, 1664.
- [6] J. C. Philp, R. J. Ritchie, J. E. M. Allan, *Trends Biotechnol.* **2013**, *31*, 219.
- [7] M. Winnacker, B. Rieger, *Macromol. Rapid Commun.* **2016**, *37*, 1391.
- [8] H. Kawaguchi, T. Hasunuma, C. Ogino, A. Kondo, *Curr. Opin. Biotechnol.* **2016**, *42*, 30.
- [9] L. Salamanca-Cardona, R. A. Scheel, B. R. Lundgren, A. J. Stipanovic, K. Matsumoto, S. Taguchi, C. T. Nomura, *Bioeng.* **2014**, *5*, 284.
- [10] H. Kawaguchi, Y. Katsuyama, D. Du, P. Kahar, S. Nakamura-Tsuruta, H. Teramura, K. Wakai, K. Yoshihara, H. Minami, C. Ogino, Y. Ohnishi, A. Kondo, *Appl. Microbiol. Biotechnol.* **2017**, *101*, 5279.
- [11] J. Tomaszewska, D. Bieliński, M. Binczarski, J. Berłowska, P. Dziugan, J. Piotrowski, A. Stanishevsky, I. A. Witońska, *RSC Adv.* **2018**, *8*, 3161.
- [12] L. Telen, P. Van Puyvelde, B. Goderis, *Macromolecules* **2016**, *49*, 876.
- [13] N. Samadi, C. F. van Nostrum, T. Vermonden, M. Amidi, W. E. Hennink, *Biomacromolecules* **2013**, *14*, 1044.
- [14] J. Rydz, W. Sikorska, M. Kyulavska, D. Christova, *Int. J. Mol. Sci.* **2015**, *16*, 564.
- [15] S.-Y. Yang, H.-X. Yang, A.-J. Hu, *Advanced Polyimide Materials: Synthesis, Characterization, and Applications*, Elsevier, New York **2018**, Ch. 4, p. 137.
- [16] W. Thielemans, R. P. Wool, *Biomacromolecules* **2005**, *6*, 1895.
- [17] A. Llevot, E. Grau, S. Carlotti, S. Grelier, H. Cramail, *Macromol. Rapid Commun.* **2016**, *37*, 9.
- [18] L. Mialon, A. G. Pemba, S. A. Miller, *Green Chem.* **2010**, *12*, 1704.
- [19] M. S. Ganewatta, H. N. Lokupitiya, C. Tang, *Polymers* **2019**, *11*, 1176.
- [20] T. Hamada, S. Hasegawa, H. Fukasawa, S. Sawada, H. Koshikawa, A. Miyashita, Y. Maekawa, *J. Mater. Chem. A* **2015**, *3*, 20983.
- [21] S. Ohashi, J. Kilbane, T. Heyl, H. Ishida, *Macromolecules* **2015**, *48*, 8412.
- [22] S. R. Kwon, J. Harris, T. Zhou, D. Loufakis, J. G. Boyd, J. L. Lutkenhaus, *ACS Nano* **2017**, *11*, 6682.
- [23] H. Shin, S. Wang, S. Tateyama, D. Kaneko, T. Kaneko, *Ind. Eng. Chem. Res.* **2016**, *55*, 8761.
- [24] M. A. Ali, T. Kaneko, *Ind. Eng. Chem. Res.* **2019**, *58*, 15958.
- [25] J. He, N. Magarvey, M. Pirae, L. C. Vining, *Microbiology* **2001**, *147*, 2817.
- [26] X. Jin, S. Tateyama, T. Kaneko, *Polym. J.* **2015**, *47*, 727.
- [27] P. Suvannasara, S. Tateyama, A. Miyasato, K. Matsumura, T. Shimoda, T. Ito, Y. Yamagata, T. Fujita, N. Takaya, T. Kaneko, *Macromolecules* **2014**, *47*, 1586.
- [28] S. Tateyama, S. Masuo, P. Suvannasara, Y. Oka, A. Miyazato, K. Yasaki, T. Teerawatananond, N. Muangsin, S. Zhou, Y. Kawasaki, L. Zhu, Z. Zhou, N. Takaya, T. Kaneko, *Macromolecules* **2016**, *49*, 3336.
- [29] Z. Qian, M. Yang, R. Li, D. Li, J. Zhang, Y. Xiao, C. Li, R. Yang, N. Zhao, J. Xu, *J. Mater. Chem. A* **2018**, *6*, 20769.
- [30] G. M. Wu, C. H. Hung, *J. Achiev. Mater. Manuf. Eng.* **2006**, *17*, 27.
- [31] Celazole PBI, <https://pbipolymer.com/celazole-pbi-products/t-series/> (accessed: March 2020).
- [32] J. Yang, D. Aili, Q. Li, Y. Xu, P. Liu, Q. Che, J. O. Jensen, N. J. Bjerrum, R. He, *Polym. Chem.* **2013**, *4*, 4768.
- [33] V. V. Korshak, M. M. Teplyakov, *J. Macromol. Sci., Part C: Polym. Rev.* **1971**, *5*, 409.
- [34] A. A. Izyneev, M. M. Teplyakov, V. G. Samsonova, A. D. Maksimov, *Russ. Chem. Rev.* **1967**, *36*, 912.
- [35] A. Choudhury, A. K. Bhowmick, C. Ong, M. Soddemann, *J. Nanosci. Nanotechnol.* **2010**, *10*, 5056.
- [36] G. H. Melton, E. N. Peters, R. K. Arisman, in *Applied Plastics Engineering Handbook* (Ed: M. Kutz), William Andrew Publishing, Oxford **2011**, pp. 7–21.
- [37] H. Suzuki, Y. Ohnishi, Y. Furusho, S. Sakuda, S. Horinouchi, *J. Biol. Chem.* **2006**, *281*, 36944.
- [38] H. Kawaguchi, K. Sasaki, K. Uematsu, Y. Tsuge, H. Teramura, N. Okai, S. Nakamura-Tsuruta, Y. Katsuyama, Y. Sugai, Y. Ohnishi, K. Hirano, T. Sazuka, C. Ogino, A. Kondo, *Bioresour. Technol.* **2015**, *198*, 410.
- [39] C. J. Arnold, *J. Polym. Sci., Part D* **1979**, *14*, 265.
- [40] D. Koma, H. Yamanaka, K. Moriyoshi, T. Ohmoto, K. Sakai, *Appl. Environ. Microbiol.* **2012**, *78*, 6203.
- [41] T. Kubota, A. Watanabe, M. Suda, T. Kogure, K. Hiraga, M. Inui, *Metab. Eng.* **2016**, *38*, 322.
- [42] Q. Xu, Y. Gao, M. Qin, K. Wu, Y. Fu, J. Zhao, *Int. J. Biol. Macromol.* **2013**, *60*, 241.
- [43] M. Marinova, E. Mateos-Espejel, N. Jemaa, J. Paris, *Chem. Eng. Res. Des.* **2009**, *87*, 1269.
- [44] W. W. Wright, *Polym. Int.* **1994**, *33*, 438.
- [45] DuPont Kapton Polyimide Films, <https://www.dupont.com/electronic-materials/kapton-polyimide-film.html> (accessed: November 2019).
- [46] P. Patel, T. R. Hull, R. E. Lyon, S. I. Stolarov, R. N. Walters, S. Crowley, N. Safronava, *Polym. Degrad. Stab.* **2011**, *96*, 12.
- [47] VICTREX High Performance PEEK Polymers. (n.d.), [https://www.victrex.com/-/media/datasheets/victrex\\_tds\\_450g.pdf](https://www.victrex.com/-/media/datasheets/victrex_tds_450g.pdf) (accessed: November 2019).
- [48] K. H. Seo, L. S. Park, J. B. Baek, W. Brostow, *Polymer* **1993**, *34*, 2524.
- [49] Matweb, *Overview of Materials for Nylon 6/66*, [http://www.matweb.com/search/datasheet\\_print.aspx?matguid=26386631ec1b49eeba62c80a49730dc4](http://www.matweb.com/search/datasheet_print.aspx?matguid=26386631ec1b49eeba62c80a49730dc4) (accessed: March 2020).
- [50] J.-J. Li, G.-J. Song, X.-L. She, P. Han, Z. Peng, D. Chen, *Polym. J.* **2006**, *38*, 554.
- [51] S. Mehdipour-Ataei, Z. Tabatabaei-Yazdi, *Heat Resistant Polymers in Encyclopedia of Polymer Science and Technology*, American Cancer Society, Atlanta, Georgia, USA **2015**, pp. 1–31.
- [52] E. P. Gaudette, *SAE Trans.* **1985**, *94*, 382.
- [53] A. B. Morgan, M. Bundy, *Fire Mater.* **2007**, *31*, 257.
- [54] A. Nag, M. A. Ali, M. Watanabe, M. Singh, K. Amornwachirabodee, S. Kato, T. Mitsumata, K. Takada, T. Kaneko, *Polym. Degrad. Stab.* **2019**, *162*, 29.
- [55] W. D. Callister, Jr., *Materials Science and Engineering: An Introduction*, 7th Edition Wiley Plus Set, John Wiley & Sons Inc., New York, USA **2006**.
- [56] E. Oberg, C. J. McCauley, F. D. Jones, H. L. Horton, H. H. Ryffel, *Machinery's Handbook: A Reference Book for the Mechanical Engineer, Designer, Manufacturing Engineer, Draftsman, Toolmaker, and Machinist*, Industrial Press, New York, USA **2012**.
- [57] F. Carrasco, P. Pagès, J. Gámez-Pérez, O. O. Santana, M. L. Maspocho, *Polym. Degrad. Stab.* **2010**, *95*, 116.
- [58] M. Koller, *Appl. Food Biotechnol.* **2014**, *1*, 3.
- [59] K.-H. Hsu, C.-W. Chen, L.-Y. Wang, H.-W. Chan, C.-L. He, C.-J. Cho, S.-P. Rwei, C.-C. Kuo, *Soft Matter* **2019**, *15*, 9710.
- [60] S. Dwivedi, T. Kaneko, *Green Polymer Chemistry: New Products, Processes, and Applications*, Washington DC, USA **2018**, 201.
- [61] H. Kawaguchi, K. Uematsu, C. Ogino, H. Teramura, S. Niimi-Nakamura, Y. Tsuge, T. Hasunuma, K.-I. Oinuma, N. Takaya, A. Kondo, *Biochem. Eng. J.* **2014**, *88*, 188.
- [62] C. Keilhauer, L. Eggeling, H. Sahm, *J. Bacteriol.* **1993**, *175*, 5595.
- [63] S. Nara, T. Komiya, *Starch/Stärke* **1983**, *35*, 407.
- [64] M.-H. Hao, *J. Chem. Theory Comput.* **2006**, *2*, 863.
- [65] C. Lee, W. Yang, R. G. Parr, *Phys. Rev. B* **1988**, *37*, 785.
- [66] Y. Tawada, T. Tsuneda, S. Yanagisawa, T. Yanai, K. Hirao, *J. Chem. Phys.* **2004**, *120*, 8425.
- [67] R. Fodil, M. Sekkal-Rahal, A. Sayede, *J. Mol. Model.* **2017**, *23*, 31.
- [68] Y. Zhao, D. G. Truhlar, *J. Phys. Chem. A* **2004**, *108*, 6908.